



Micropatterning of diamond crystallites via cobalt-catalyzed thermochemical etching

Junsha Wang^{1,2}, Long Wan^{1,*} , Jing Chen¹, and Jiwang Yan²

¹College of Materials Science and Engineering, Hunan University, Changsha 410082, People's Republic of China

²Department of Mechanical Engineering, Keio University, Yokohama 223-8522, Japan

Received: 30 June 2016

Accepted: 1 September 2016

Published online:

8 September 2016

© Springer Science+Business Media New York 2016

ABSTRACT

In this paper, we report a thermochemical etching method to fabricate well-distributed micropatterns with large pattern ratios on diamond crystallites using cobalt (Co) powder. The effect of temperature on the depth and area of the micropatterns on different crystal planes is quantified. Results show that the depth and area of the patterns on the same plane increase with the temperature and that, at the same processing temperature, the pattern depth and area on {100} planes are larger than those on {111} planes. After heat treatment at 850 °C, the pattern depths on {100} and {111} planes reach 4.0 and 3.5 μm, and the corresponding average ratios of the pattern area are 54 and 46 %, respectively. The morphologies of the micropatterns on (001), (113), (101), and (111) planes are dependent on the relative orientations between the etched crystal plane and its adjacent planes, and diamond nanoparticles with specific orientations are observed on etched {100} planes. Furthermore, graphite is detected in the etch patterns, suggesting that thermochemical etching process involves the phase transformation from diamond to graphite.

Introduction

Synthetic diamond possesses outstanding properties, such as superior hardness, high wear resistance, and high heat conductivity, thereby making them preferable for machining hard and brittle materials [1, 2]. However, given the small size of the diamond crystallites, binder materials are usually required to bond them together to form diamond tools with specific size, shape, and strength. To prevent the graphitization of diamond, the sintering of diamond

tools must be performed below a critical temperature [3]. Thus, the adhesion strength between diamond grains and binder materials is very weak. Additionally, the smooth diamond surface is chemically inert to binder materials, which in turn reduces the adhesion strength at the interface. Consequently, diamond grains prematurely fall off from the tool surface before real machining. To improve the adhesion strength between diamond and binder materials, a series of research was conducted about diamond surface coating [4–7]. Some metal coatings (Ti, Cr, etc.) can be chemically bonded with diamond,

Address correspondence to E-mail: wanlong1799@163.com

whereas others (Cu, Ni, etc.) are only mechanically coated on the surface. In the latter case, diamond particles are pulled out by machining force, whereas the coating layers are retained in the binder. Moreover, the thick ductile metal layer reduces the self-sharpening ability of diamond cutting edges and increases the power consumption during machining.

To increase the adhesion strength effectively, this study proposes to fabricate micropatterns on diamond surface. After patterning, the effective contact area between diamond and the binder is greatly expanded. Moreover, the micropatterns can serve as “anchors” to increase the retention capability of binders to diamond grains.

As a typical method of diamond etching, catalytic gasification has been used to etch diamond thin films for chemical sensors [8]. Thin metallic layers are deposited on diamond by evaporation, and metal nanoparticles are generated after heat treatment in flowing hydrogen gas. After etching, the largest size of the nanopores that forms on the thin diamond film is 225 nm. To study the action of iron particles at catalyzed hydrogenation of synthetic diamond, iron particles were directly loaded on diamond surface [9, 10]. The evolution of iron particles on different crystal planes was investigated, but the extent of etching was not evaluated. Iron nitrate was loaded on diamond crystallites surface by impregnation, and the etching behavior at 900 °C in a flowing gas mixture of H₂ (10 %) + N₂ (90 %) was investigated [11]. It is found that the etching behavior was highly dependent not only on the crystal plane of diamond, but also on the loading amount of iron. Due to the uneven distribution of iron nitrate, the extent of etching on diamond varied greatly from particle to particle. Using the same method, the etching behaviors on {100} and {111} planes by cobalt nanoparticles were analyzed [12]. However, the formation of nanopatterns was at the sacrifice of the disappearance of the original diamond surface.

The above literatures suggest that although a modicum of success has been attained in diamond film surface patterning, methods to form well-dispersed micropatterns on all planes of diamond crystallites with the original surface retained were not yet reported. In previous papers, we attempted to pattern diamond crystallites by iron and nickel powder without using flowing hydrogen [13, 14]. The etching phenomena of diamond by iron was verified, but the original crystal surface was easily etched away.

Although micropatterns were achieved by nickel etching, the ratios of pattern area to the original surface were quite low. Until 950 °C, the percentages on {100} and {111} planes are only 21 and 9 %, respectively. Compared to nickel, cobalt shows better wettability toward to diamond [15, 16]. Thus, well-distributed micropatterns with higher pattern ratios are expected from small-sized cobalt powder etching. Under the thermochemical catalytic effect of cobalt, patterning performance on diamond surface was investigated. By adjusting the etching temperature, the quantitative control of the area and depth of the patterns on different crystal planes was attempted. Moreover, the evolution of anisotropic patterns and nanoparticles on etched {100} planes were analyzed.

Experimental

Materials

Synthetic diamond particles (LD 240) with an average diameter of approximately 500 μm were commercial obtained from Henan Liliang New Material Co., Ltd., Zhengzhou, China. Cobalt powder with size distribution of 4–8 μm was commercial obtained from Zhuzhou Cemented Carbide Works, Zhuzhou, China. Concentrated hydrochloric acid (HCl), nitric acid (HNO₃), sulfuric acid (H₂SO₄), and perchloric acid (HClO₄) were purchased from Changsha Tianheng Scientific Instrument & Equipment Co., Ltd., Changsha, China.

Micropatterning process

The synthetic diamond particles and cobalt powder were mixed at a ratio of 1: 13 (weight). The mixture was then wrapped by graphite paper and moved to a graphite crucible with carbon black at the bottom. To facilitate close contact between diamond and cobalt, the mixture was compacted by hand. The graphite crucible was then filled with carbon black. To avoid the effect of air, the graphite crucible containing the sample was buried in an airtight ceramic crucible full of carbon black. Finally, the ceramic crucible was moved to a muffle furnace and was heated at a rate of 3 °C/min from room temperature to 600 °C followed by 2 °C/min to 750 °C. The heating rate was then changed to 1.5 °C/min up to the objective temperature and was retained for 1 h. After heat treatment,

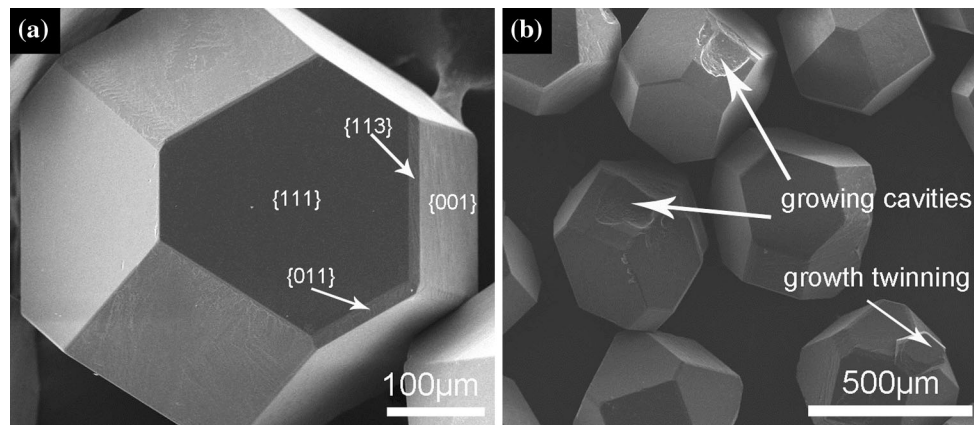


Figure 1 Morphology of **a** a well-grown diamond crystallite and **b** growth defects in diamond.

the sample was washed with aqua acid (HNO_3 : $\text{HCl} = 1: 3$, volume ratio) to remove the metal.

Characterization

The morphologies of the diamond crystallites were observed using an environment scanning electron microscope (ESEM, FEI, Inspect S50) and field-emission scanning electron microscope (FESEM, FEI, Sirion). The percentages of the pattern area were measured with a white-light interferometer (Taylor Hobson Ltd., CCI 1000), and the pattern depths were detected via laser-probe surface profiling (Mitaka Kohki Corporation, MP-3). The elements on the diamond surface were analyzed by energy dispersive X-ray spectroscopy (EDX, Bruker, XFlash Detector 4010). The phase changes of diamond and cobalt during etching were characterized by X-ray diffraction (XRD, Bruker, D8 Advance) with $\text{Cu K}\alpha$ radiation and micro-Raman (JASCO Corporation, NRS-3100YM, 532 nm, laser spot size: 1 μm), respectively.

Results and discussion

Micropatterns on the diamond surface

The untreated synthetic diamond particles were grown under high pressure and high temperature. As Fig. 1(a) shows, a well-grown diamond crystallite typically assumes the form of a hex-octahedron, consisting of six $\{100\}$ planes and eight $\{111\}$ planes. Due to the temperature or pressure fluctuations, or accumulation of impurities on the interface, secondary $\{011\}$ and $\{113\}$ planes are occasionally visible [17]. Moreover, growth defects, such as growing cavities or

twinning, also appear on the diamond surface [18, 19]. The area of $\{111\}$ planes is always the largest, which suggests that $\{111\}$ planes are the most stable and slowest growing facets among all the planes.

To fabricate micropatterns on the diamond surface, the mixture of diamond and cobalt was heated at a temperature range of 600–950 $^\circ\text{C}$. After the metal was washed away, the morphologies of the diamond particles were observed, as shown in Fig. 2. Figure 2(a2) clearly shows that the orthogonal microchannels aligned in $\langle 100 \rangle$ direction are formed on $\{100\}$ planes. However, the orientations of the sides change to $\langle 110 \rangle$ direction at the end of the channels [indicated by the square in Fig. 2(a2)]. For $\{111\}$ planes of diamond, only a few micropatterns are observed, and their orientations are irregular. When treated at 700 $^\circ\text{C}$, micropatterns with flat bottom develop on $\{111\}$ planes, and the number increases remarkably. By contrast, reversed pyramids or channels with $\langle 110 \rangle$ edges are found on $\{100\}$ planes. After the temperature rises to 800 $^\circ\text{C}$, the size and depth of the patterns on both $\{100\}$ and $\{111\}$ planes increase dramatically. As a result, micropatterns can be easily distinguished even at a lower magnification, as shown in Fig. 2(c1). When heated at 900 $^\circ\text{C}$, the patterns on $\{100\}$ planes connect together, thereby leading to the disappearance of the etch pits. By contrast, $\{111\}$ planes are characterized by hexagons with flat bottom.

Figure 3 shows the depth of the patterns with an increase in the temperature. As shown in figure, the depth of the patterns on both $\{100\}$ and $\{111\}$ planes increases with an increase in the treatment temperature. This may derive from the influence of temperature on the stability of diamond carbon atoms and the solubility of carbon in cobalt. With an increase in

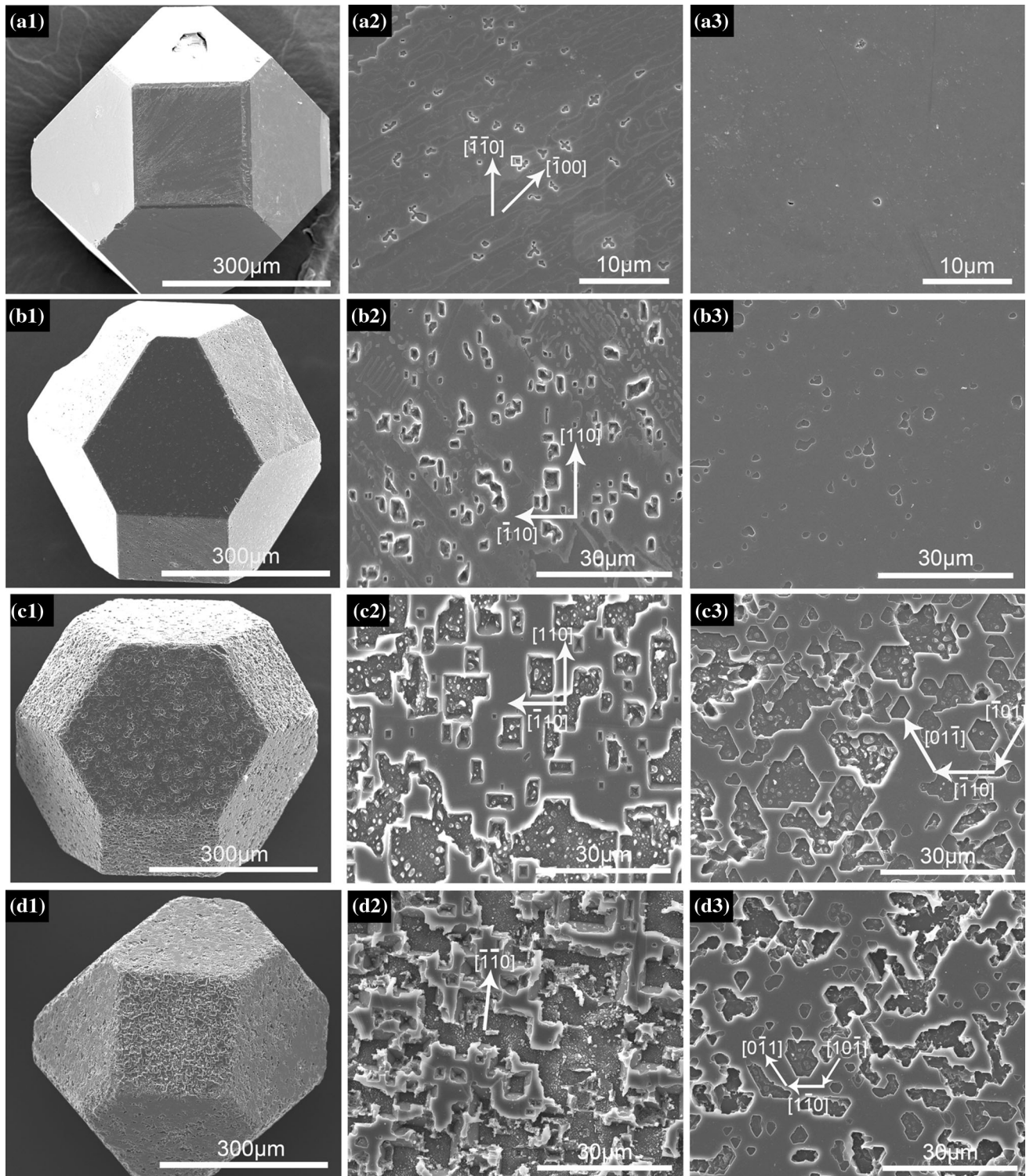


Figure 2 Morphology of diamond crystallites heated at **a1** 600 °C, **b1** 700 °C, **c1** 800 °C, and **d1** 900 °C. **a2**, **b2**, **c2**, and **d2** are the corresponding {100} planes, and **a3**, **b3**, **c3**, and **d3** are the corresponding {111} planes.

temperature, the stability of diamond carbon decreases, and the solubility of carbon in cobalt increases [20]. Thus, carbon atoms can easily escape

from the diamond structure and diffuse into the vacant sites in cobalt. Given that {111} planes in diamond are the closest packing planes, larger

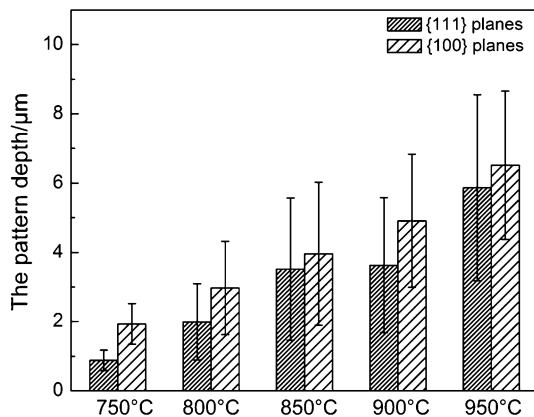


Figure 3 Depth of patterns with increased temperature.

activation energy is required to destroy the diamond structure. Thus, the patterns on {111} planes are shallower than those on {100} planes at the same temperature. Treated at 850 °C, the difference in pattern depth on {111} and {100} planes is the smallest, which is 3.5 and 4.0 μm, respectively.

The ratios of the pattern areas at different temperatures are recorded in Fig. 4, which exhibits the same trend as the depth of patterns. The melting point of cobalt bulk is 1493 °C. Given the size effect, molten cobalt particles can form on the diamond surface at 800 °C, as shown in Fig. 1S. With an increase in temperature, the melting degree of cobalt increases, resulting in the aggregation of small cobalt particles. Consequently, the wetting area, reflected by the pattern area, increases with the temperature. The difference between {100} and {111} planes may be caused by the surface energy [21]. The surface energy of {100} planes is higher than that of {111} planes.

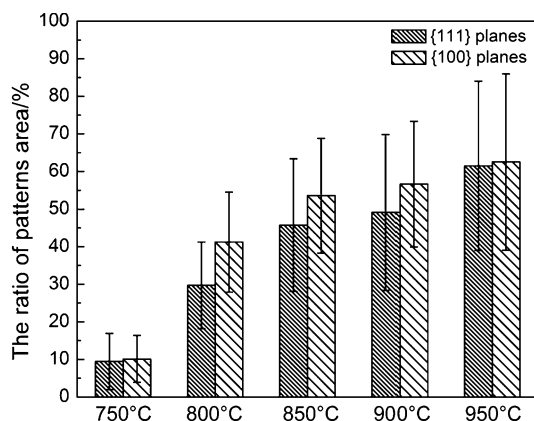


Figure 4 Ratios of the pattern areas at different temperatures.

According to Young's equation [22], a smaller contact angle is achieved between {100} planes and metals. Thus, at the same temperature, the pattern area on {100} planes is larger than that on {111} planes. At 850 °C, the average ratios of the pattern area on {100} and {111} planes are quite close, which are 54 and 46 %, respectively.

Anisotropy of micropatterns

Under high temperature and high pressure, diamond can be synthesized from graphite with the help of ferrous metals. However, these metals also catalyze the transition from diamond to graphite in the stability field of graphite at low pressure [23, 24]. As a result, the morphology of the micropatterns on the diamond plane reflects the characteristics of this plane and its interrelationships with adjacent planes.

The micropatterns that developed on different crystal planes at 750 °C are shown in Fig. 5. On (001) plane, reversed four-sided pyramids with rough bottoms are formed. Occasionally, traces of steps are visible on the sidewalls [as shown in Fig. 2S(a)]. The patterns on (113) plane are tetrahedrons with the outline of isosceles trapezoids. The morphology of (101) plane is characterized by elongated hexagonal channels. For (111) plane, hexagons with flat bottoms develop, and layer-like structures are observed on the sidewalls. In a deep etch pit formed at 850 °C [shown in Fig. 2S(b)], smooth sidewalls and rough sidewalls form with an alternating arrangement, which indicates that the crystallographic indices of the sidewalls are not the same.

According to the periodic bond chain (PBC) theory [25], {111} planes made up of three PBC vectors are the only flat planes (*F*-planes), whose growth rate is the slowest. Other planes with one or zero PBC vector are rough surfaces, which are supposed to be invisible. However, under (2 × 1) surface reconstruction, {100} planes also can behave like *F*-faces and always appear on the diamond surface [26, 27]. As for {011} and {113} planes, they are transient faces and are only occasionally visible. In a word, the stability order of diamond crystal planes can be expressed as {111} > {100} » {110} ≈ {113}. Thus, although {113} planes are the nearest neighbor planes of the (001) plane, etch pits on (001) plane are bounded by its secondary adjacent {111} planes. For the same reason, the rough and smooth sidewalls of the patterns on (111) plane in Fig. 2S(b) correspond to {100} and {111}

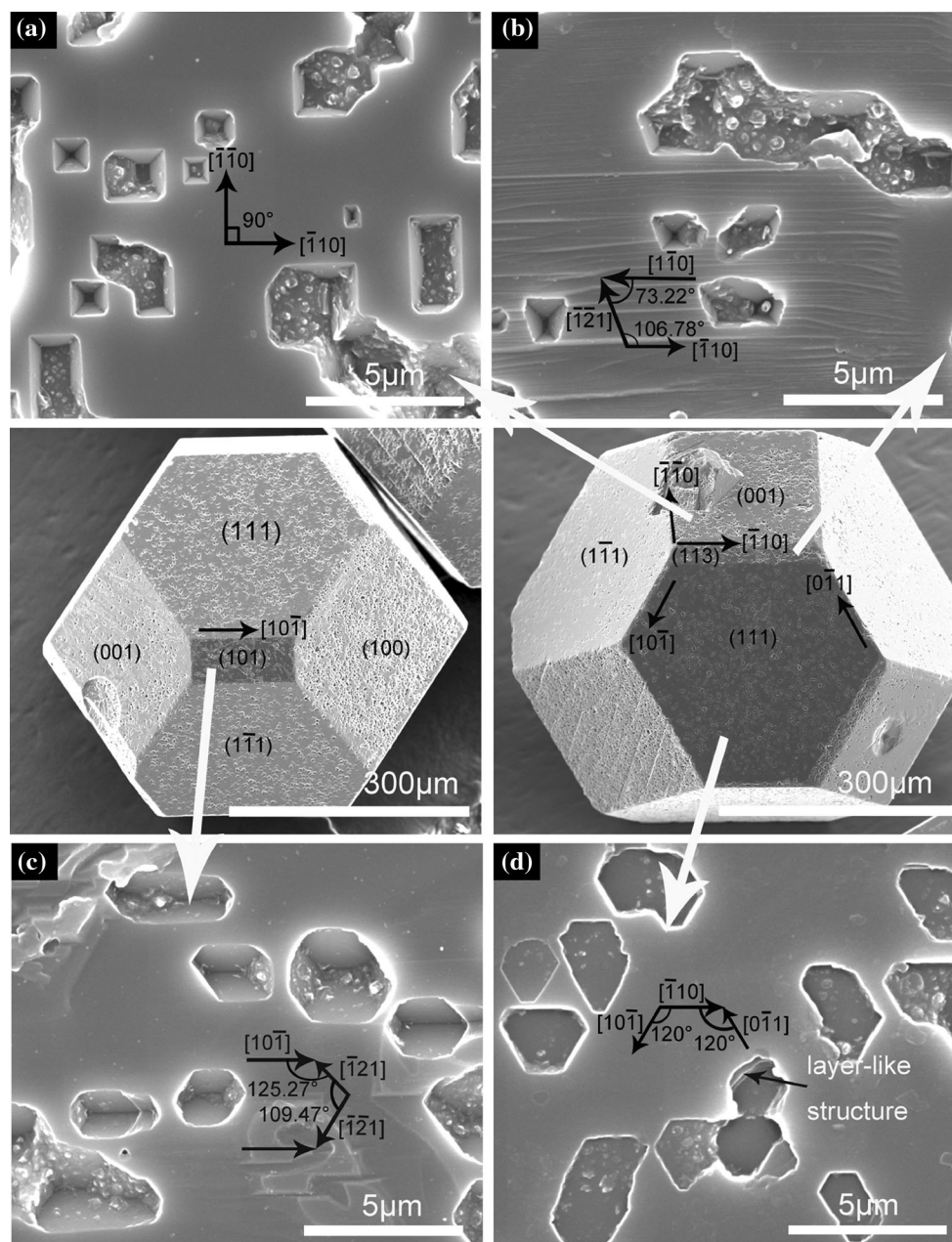
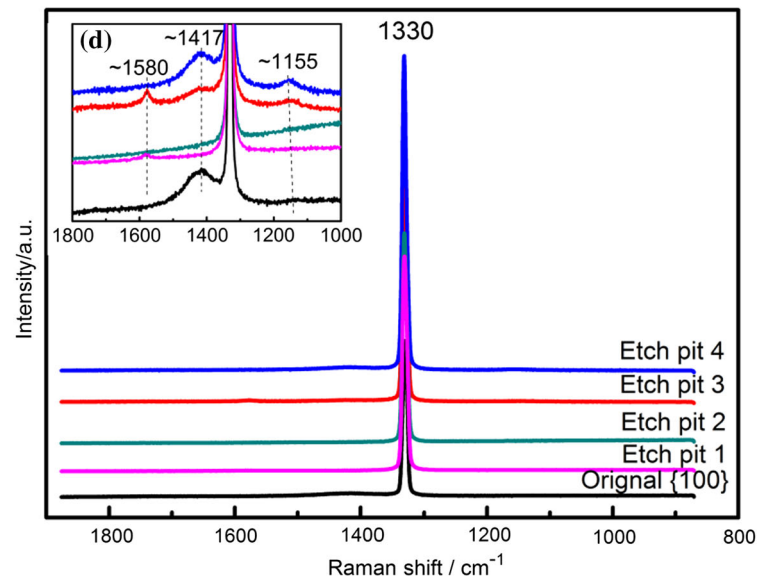
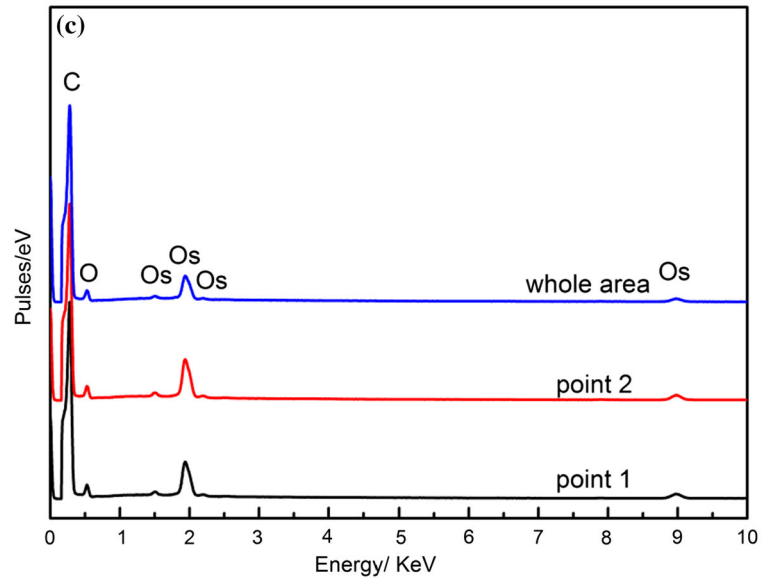
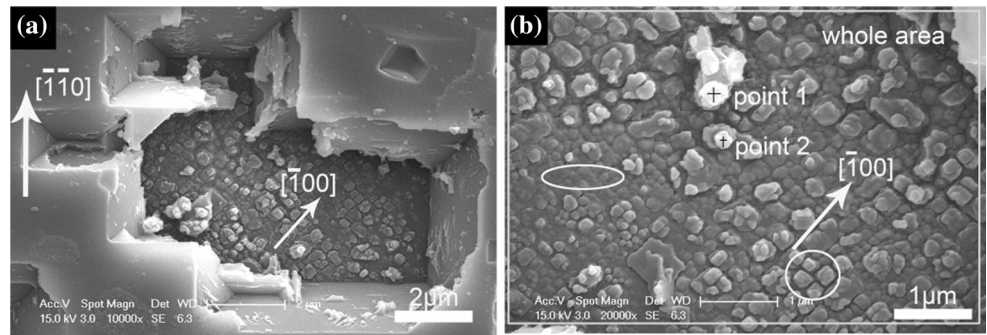


Figure 5 Micropatterns on **a** (001) plane, **b** (113) plane, **c** (101) plane, and **d** (111) plane formed at 750 °C.

planes, respectively. Being different from Takasu's results [12], the sidewalls of patterns on (111) plane are not perpendicular to their bases. To analyze the morphology of the micropatterns on the transient (101) and (113) planes, a diamond crystallite with well-developed {113} and {101} planes is used as the model [28]. In this model, (101) plane is surrounded by two {111} planes and four {113} planes. Due to the stability of its secondary adjacent {100} planes is higher than {113} planes, thus they develop as the steeping planes at the ends of patterns on (101) plane.

Similarly, patterns on (113) plane are stopped by its secondary adjacent {111} planes. Based on the identified indices of the crystal planes inside the patterns, the edge orientations of the patterns are calculated. Interestingly, almost all the sides of the patterns on {100} and {111} planes are shown to be aligned in the $\langle 110 \rangle$ direction, which is similar to the result of diamond etching in liquid nitrate [29] and by oxygen above 775 °C [30]. This is because $\langle 110 \rangle$ direction contains strong bond and requires larger energy to break than other directions. Furthermore, traces of

Figure 6 Analysis of diamond heated at 900 °C and washed by aqua regia: **a** and **b** FESEM image of micropatterns on {100} planes, **c** EDAX spectra, and **d** micro-Raman spectra.

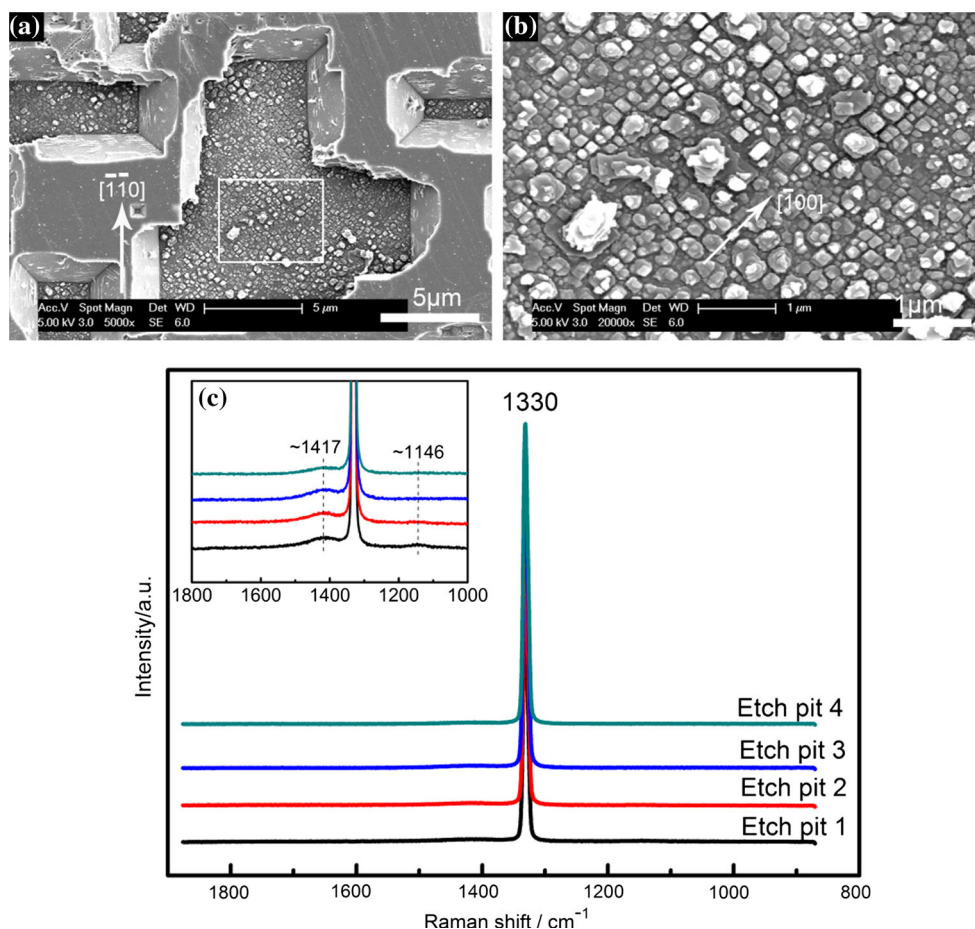


steps or layer-like structures are observed on the sidewalls of the patterns [Figs. 2S, 5(d)], which indicates that the etching on *F*-planes or *F*-like planes proceeds by a step mode.

Nanoparticles on the etched {100} planes

Figures 2 and 5 show that the bottom of the patterns on {100} planes is rough, whereas that on {111} planes

Figure 7 Analysis of diamond heated at 900 °C and washed with aqua regia and mixed acid (H_2SO_4 : HClO_4 : $\text{HNO}_3 = 5: 3: 1$): **a** FESEM image of the micropatterns on {100} planes, **b** enlarged part of square in (a), and **c** micro-Raman spectra.



tends to be smooth. To observe the rough etch bottom on {100} planes more clearly, the microstructure of the micropatterns formed at 900 °C was examined under high magnification. Figure 6a, b shows that the bottom of the patterns on {100} planes is covered with nanoparticles. Some particles [indicated by the ellipse in Fig. 6(b)] are irregular and continuous, similar to the morphology of nanocrystalline diamond film [31]. By contrast, some particles [indicated by the circle in Fig. 6(b)] are regular squares with edges oriented in the $\langle 100 \rangle$ direction. To analyze the element and the phase of the nanoparticles, the patterns on {100} planes are characterized by EDX and micro-Raman. The EDX results show that the Co element is absent. Sharp diamond peaks at 1330 cm^{-1} [32] and $sp^3 \text{ CH}_2$ peaks at 1417 cm^{-1} [33] are identified in the micro-Raman spectra. Moreover, sp^2 carbon peaks at 1580 cm^{-1} [34] and nanodiamond peaks at 1155 cm^{-1} [31, 35] are also detected. These results indicate that the nanoparticles inside the patterns on {100} planes are mainly composed of graphite or nanodiamond.

To exclude the possibility of graphite, the diamond particles were washed with aqua regia, followed by mixed acid (H_2SO_4 : HClO_4 : $\text{HNO}_3 = 5: 3: 1$). Figure 7a, b shows that the morphologies of the nanoparticles before and after washing in mixed acid do not differ. While in the micro-Raman spectra, the graphite peak disappears, indicating that graphite is decomposed by the mixed acid. Weak peaks around 1146 cm^{-1} still exist, showing the high possibility that the particles at the bottom of the patterns on {100} planes are nanodiamond.

Etching mechanism

To investigate the phase changes during the etching process, the XRD patterns of diamond and cobalt powder before and after heating at 900 °C are compared in Fig. 8. In the structure of the as-received diamond particles, the inclusion ($\text{CFe}_{2.5}$) is trapped inside. By contrast, cobalt powder is a pure metal that consists of two types of crystal structure: cubic and hexagonal system. After the mixture was heated,

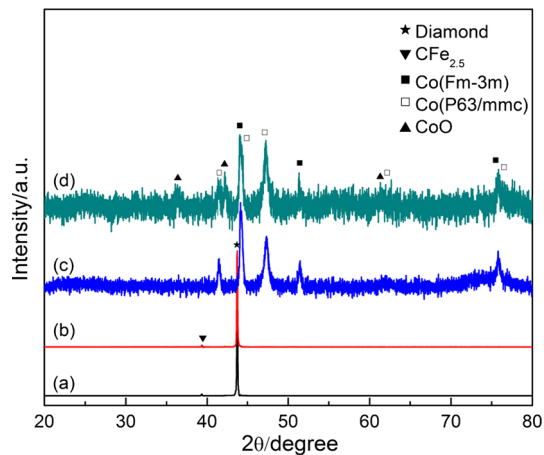


Figure 8 XRD patterns of *a* pristine diamond, *b* Co-patterned diamond before acid wash, *c* pristine cobalt powder, and *d* cobalt powder separated from the diamond-cobalt bulk after experiment.

diamond and cobalt were separated and then tested by X-ray diffraction. In the spectra of the diamond particles, neither graphite nor cobalt is detected. Although weak CoO peaks are identified in the

spectra of metal powder, most of the cobalt powder remains as pure metal.

The oxidation of cobalt results in the formation of CoO but not Co₃O₄, demonstrating that the amount of oxygen is insufficient. Such oxidation reaction may occur in the etching process or preservation process after the experiment. If the former is the case, then the oxygen should come from the sample preparation process. To clarify whether or not the residual oxygen has an effect on diamond etching, the diamond was buried in the carbon black and then heated at 900 °C. From the morphology shown in Fig. 9(a), little changes are observed on the diamond surface. It means that the oxygen in the reaction zone is too little to cause the oxidation of diamond. To investigate the possibility of oxidation–reduction reaction between diamond and cobalt, the Gibbs energy of various reactions versus temperature is calculated. As suggested in Fig. 3S, the initial oxidation–reduction reaction temperature should be dependent on the amount of oxygen. When the oxygen is deficient, the reaction occurs above 213 °C (486 K). To

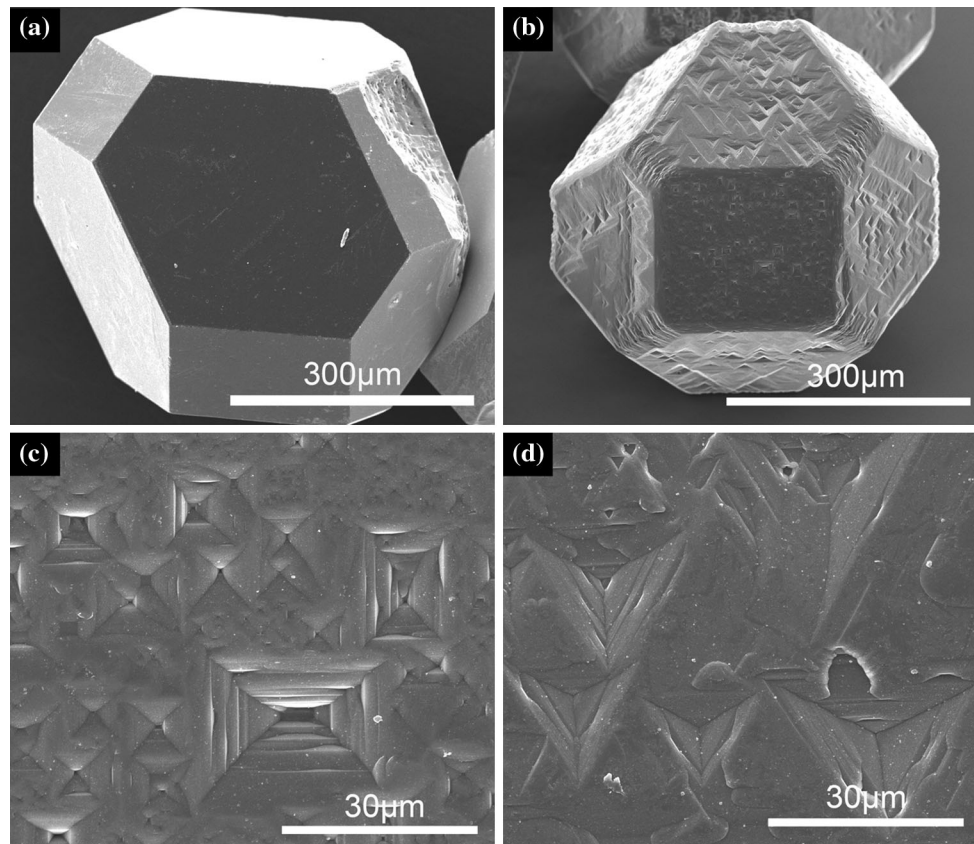


Figure 9 Morphology of diamond: *a* diamond buried in carbon black heated at 900 °C, *b* diamond and nickel exposed in air and heated at 900 °C, *c* and *d* {100} and {111} planes corresponding to (b).

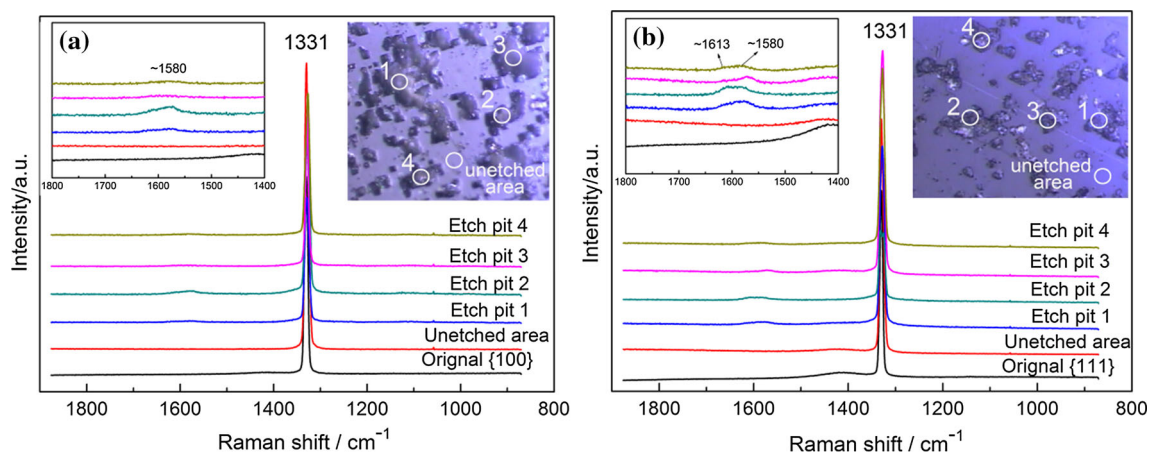


Figure 10 Raman spectrum of the Co-patterned diamond surface before acid wash: **a** {100} planes and **b** {111} planes.

verify this experimentally, the mixture of diamond and cobalt was exposed to air and then heated at 900 °C. Diamond and cobalt were tested by XRD separately, as shown in Fig. 4S. After heat treatment in air, only Co_3O_4 and CoO are detected in the cobalt powder. However, no new material is found on the diamond. The morphology of diamond in Fig. 9(c) shows that {100} planes lose their original appearance and change into reversed pyramids with interlaced steps. By contrast, “positive” trigons are observed on {111} plane, which is similar to the diamond surface etched in $\text{O}_2/\text{H}_2\text{O}$ [36] and potassium nitrate [37]. Because the morphologies of diamond in Fig. 2 processed in carbon black do not show the traces of etching characteristics in air, the synergistic effect of oxygen and cobalt on the formation of patterns can be ignored.

To analyze the phase of carbon, the etched diamond surface before acid washing was examined using micro-Raman, as shown in Fig. 10. On {100} and {111} planes, unetched areas, similar to the original surface, are characterized by sharp diamond peaks (1331 cm^{-1}). Inside the patterns, graphite carbon peaks (1580 cm^{-1}) are detected. It means that the phase transformation from diamond to graphite is involved in the diamond patterning process.

In the cobalt structure (Fig. 5S), the edge length of the equilateral triangle formed by the three adjacent atoms on (111) plane is 2.51 \AA , and that of three atoms in the diamond structure is 2.52 \AA . Given that their edge lengths are very close, Co atoms on (111) plane can be vertically aligned with diamond atoms. As shown in Fig. 6S, three Co atoms are vertically

aligned with diamond atoms 1, 3, and 5. With three unpaired d electrons, Co atoms attract the electrons of diamond atoms 1, 3, and 5 and simultaneously compress atoms 2, 4, and 6. The diamond structure is then converted into a hexagonal graphite structure.

Conclusions

A thermochemical etching method to fabricate micropatterns on diamond crystallites using cobalt is proposed. Temperature has a strong effect on the etching behavior. The higher the temperature is, the larger the pattern depth and area. At the same temperature, the pattern depth and area on {100} planes are larger than those on {111} planes. At 850 °C, the extent of etching on {100} and {111} planes reaches their closest point. The average ratios of the pattern areas are 54 and 46 %, and the corresponding pattern depths are 4.0 and 3.5 μm , respectively. Reversed pyramids, tetrahedrons, elongated six-sided channels, and hexagons are formed on (001), (113), (101), and (111) planes, respectively. The analysis of morphology shows that micropatterns are bounded by the etched crystal plane and its adjacent planes. Diamond nanocells aligned in $\langle 100 \rangle$ direction are found on {100} planes. Moreover, graphite is detected in the etch patterns, indicating that the phase transformation from diamond to graphite occurred during the etching process. The proposed micropatterning method for polyhedral diamond crystallites is simple, reliable and does not require the use of especial gas.

Acknowledgements

This work was supported by the National Natural Science Foundation of China (NSFC, Grant No. 51375157). The first author (J. S. W.) would also like to acknowledge the China Scholarship Council (CSC) for providing her exchange scholarship for Ph.D. study and research at Keio University.

Electronic supplementary material: The online version of this article (doi:[10.1007/s10853-016-0365-y](https://doi.org/10.1007/s10853-016-0365-y)) contains supplementary material, which is available to authorized users.

References

- [1] Witzendorff PV, Stompe M, Moalem A, Cvetkovic S, Suttman O, Overmeyer L, Rissing L (2014) Dicing of hard and brittle materials with on-machine laser-dressed metal-bonded diamond blades. *Precis Eng* 38:162–167
- [2] Guo B, Zhao Q (2015) Wheel normal grinding of hard and brittle materials. *Int J Adv Manuf Tech* 79:1–8
- [3] Sun YX, Tsai YT, Lin KH (2015) The influence of sintering parameters on the mechanical properties of vitrified bond diamond tools. *Mater Design* 80:89–98
- [4] NIAZI AR, Shu-Kui LI, Wang YC, Liu JX, Zhi-Yu HU, Usman Z (2014) Parameters optimization of electroless deposition of Cu on Cr-coated diamond. *T Nonferr Metal Soc* 24:136–145
- [5] Xi X, Miao H, Zhang R, Cheng J (2016) Effect of phosphorus content on the properties of Ni–P coated diamond. *Surf Coat Tech* 297:27–33
- [6] Wang YH, Zang JB, Wang MZ, Zheng YZ (2003) Relationship of interface microstructure and adhesion strength between Ti coating and diamond. *Key Eng Mater* 250:41–45
- [7] Tan LR, Wang YH, Zang JB, Zhang JH (2009) Electroplating nickel–iron alloy on the diamond surface. *Key Eng Mater* 416:164–167
- [8] Mehedi H-A, Hébert C, Ruffinatto S, Eon D, Omnès F, Gheeraert E (2012) Formation of oriented nanostructures in diamond using metallic nanoparticles. *Nanotechnology* 23:455302
- [9] Chepurov AI, Sonin VM, Dereppe JM (2000) The channeling action of iron particles in the catalyzed hydrogenation of synthetic diamond. *Diam Relat Mater* 9:1435–1438
- [10] Sonin VM, Chepurov AI, Fedorov II (2003) The action of iron particles at catalyzed hydrogenation of 100 and 110 faces of synthetic diamond. *Diam Relat Mater* 12:1559–1562
- [11] Ohashi T, Sugimoto W, Takasu Y (2012) Catalytic etching of synthetic diamond crystallites by iron. *Appl Surf Sci* 258:8128–8133
- [12] Konishi S, Ohashi T, Sugimoto W, Takasu Y (2006) Effect of the crystal plane on the catalytic etching behavior of diamond crystallites by cobalt nanoparticles. *Chem Lett* 35:1216–1217
- [13] Wang J, Wan L, Chen J, Yan J (2015) Anisotropy of synthetic diamond in catalytic etching using iron powder. *Appl Surf Sci* 346:388–393
- [14] Wang J, Wan L, Chen J, Yan J (2016) Surface patterning of synthetic diamond crystallites using nickel powder. *Diam Relat Mater* 66:206–212
- [15] Naidich YV, Kolesnichenko GA (1965) Investigation of the Wetting of and Adhesion to Graphite and Diamond by Liquid Metals. *Surface Phenomena in Metallurgical Processes*. Springer, New York, pp 218–223
- [16] Andreyev AV (1994) The wetting and bonding of diamond films by high melting point metals in the range of diamond thermodynamic stability. *Diam Relat Mater* 3:1262–1264
- [17] Kanda H, Ohsawa T, Fukunaga O, Sunagawa I (1989) Effect of solvent metals upon the morphology of synthetic diamonds. *J Cryst Growth* 94:115–124
- [18] Spitsyn B, Bouilov L, Derjaguin B (1981) Vapor growth of diamond on diamond and other surfaces. *J Cryst Growth* 52:219–226
- [19] Wild C, Kohl R, Herres N, Müller-Sebert W, Koidl P (1994) Oriented CVD diamond films: twin formation, structure and morphology. *Diam Relat Mater* 3:373–381
- [20] T. Lyman, *Metallography, Structures and Phase Diagrams, Metals Handbook, Metallography Structures & Phase Diagrams*, 8 (1973)
- [21] Takai T (1985) Reconstruction and energetics for surfaces of silicon, diamond and β -SiC. *Surf Sci Lett* 164:341–352
- [22] Tanaka T, Ikawa N, Tsuwa H (1981) Affinity of diamond for metals. *CIRP Ann-Manuf Tech* 30:241–245
- [23] Bundy F, Bassett W, Weathers M, Hemley R, Mao H, Goncharov A (1996) The pressure-temperature phase and transformation diagram for carbon; updated through 1994. *Carbon* 34:141–153
- [24] CHEN, Yiqing (2007) Polishing of polycrystalline diamond composites
- [25] Hartman P, Perdok W (1955) On the relations between structure and morphology of crystals. I. *Acta Crystallogr* 8:49–52
- [26] Giling L, Van Enkevort W (1985) On the influence of surface reconstruction on crystal growth processes. *Surf Sci* 161:567–583
- [27] Van Enkevort W, Janssen G, Schermer J, Giling L (1995) Step-related growth phenomena on exact and misoriented

- 001 surfaces of CVD-grown single-crystal diamonds. *Diam Relat Mater* 4:250–255
- [28] Silva F, Achard J, Brinza O, Bonnin X, Hassouni K, Anthonis A, De Corte K, Barjon J (2009) High quality, large surface area, homoepitaxial MPACVD diamond growth. *Diam Relat Mater* 18:683–697
- [29] Khokhryakov AF, Palyanov YN (2007) Revealing of planar defects and partial dislocations in large synthetic diamond crystals by the selective etching. *J Cryst Growth* 306:458–464
- [30] De Theije F, Van Der Laag N, Plomp M, Van Enkevort W (2000) A surface topographic investigation of 001 diamond surfaces etched in oxygen. *Philos Mag A* 80:725–745
- [31] Chen YC, Tzeng Y, Cheng AJ, Dean R (2008) Inkjet printing of nanodiamond suspensions in ethylene glycol for CVD growth of patterned diamond structures and practical applications. *Diam Relat Mater* 18:146–150
- [32] Hird J, Bloomfield M, Hayward I (2007) Investigating the mechanisms of diamond polishing using Raman spectroscopy. *Philos Mag* 87:267–280
- [33] Veres M, TÓT S, Perevedentseva E, Karmenyan A, KoÓS M (2009) Raman Spectroscopy Of Uncd Grain Boundaries. *Nanostructured Materials for Advanced Technological Applications*. Springer, Heidelberg, pp 115–121
- [34] Nemanich RJ, Solin SA (1979) First- and second-order Raman scattering from finite-size crystals of graphite. *Phys Rev B* 20:392–401
- [35] Sharda T, Umeno M, Soga T, Jimbo T (2000) Growth of nanocrystalline diamond films by biased enhanced microwave plasma chemical vapor deposition: a different regime of growth. *Appl Phys Lett* 77:4304–4306
- [36] De Theije F, Van Veenendaal E, Van Enkevort W, Vlieg E (2001) Oxidative etching of cleaved synthetic diamond 111 surfaces. *Surf Sci* 492:91–105
- [37] De Theije F, Roy O, van Der Laag N, Van Enkevort W (2000) Oxidative etching of diamond. *Diam Relat Mater* 9:929–934